Understanding the interface between silicon-based materials and water: Molecular-dynamics exploration of infrared spectra

Cite as: AIP Advances **7**, 115105 (2017); https://doi.org/10.1063/1.4999086
Submitted: 04 August 2017 . Accepted: 30 October 2017 . Published Online: 07 November 2017

José A. Martinez-Gonzalez, Niall J. English, and Aoife A. Gowen

Understanding the interface between silicon-based materials and water: Molecular-dynamics exploration of infrared spectra

José A. Martinez-Gonzalez,[1,2,a] Niall J. English,[2,a] and Aoife A. Gowen[1]
[1]*School of Biosystems and Food Engineering, University College Dublin, Belfield, Dublin, Ireland*
[2]*School of Chemical & Bioprocess Engineering, University College Dublin, Belfield, Dublin, Ireland*

(Received 4 August 2017; accepted 30 October 2017; published online 7 November 2017)

Molecular-dynamics simulations for silicon, hydrogen- and hydroxyl-terminated silicon in contact with liquid water, at 220 and 300 K, display water-density 'ordering' along the laboratory z-axis, emphasising the hydrophobicity of the different systems and the position of this first adsorbed layer. Density of states (DOS) of the oxygen and proton velocity correlation functions (VACFs) and infrared (IR) spectra of the first monolayer of adsorbed water, calculated via Fourier transformation, indicate similarities to more confined, ice-like dynamical behaviour (redolent of ice). It was observed that good qualitative agreement is obtained between the DOS for this first layer in all systems. The DOS for the lower-frequency zone indicates that for the interface studied (i.e., the first layer near the surface), the water molecules try to organise in a similar form, and that this form is intermediate between liquid water and ice. For IR spectra, scrutiny of the position of the highest-intensity peaks for the stretching and bending bands indicate that such water molecules in the first solvating layer are organised in an intermediate fashion between ice and liquid water.
https://doi.org/10.1063/1.4999086

I. INTRODUCTION

The study of aqueous solutions in contact with different types of materials and bio-materials has become a subject of substantial interest, addressing open questions relating to how water organisation changes depending on the hydrophobicity of the surface. Water in close contact with surfaces of these materials, called interfacial water, plays important roles in biology,[1] meteorology,[2] geology,[3] and nanotechnology. For example, liquid water behaviour as it comes in contact with a solid surface is an interfacial phenomenon that helps us to understand membrane channels.[4] Also, water organisation, together with surface chemistry, influences many biological phenomena, such as bio-adhesion.[1,5]

The level of organisation for these interfacial water molecules is key to discerning wetting phenomena.[6] Furthermore, such interfaces provide a rich environment for unravelling how confinement of water molecules' motion is affected by the properties of the material, which can be observed in the variation of transport and vibrational properties. In addition, understanding the role of hydrogen bonding between interfacial water molecules and the surface/bulk of water is important to reveal more clues about wetting phenomena.

Silicon and silicon-based materials have been widely used in the semi-conductors industry.[7] However, in recent years, silica,[8] silicon[9] and silicon-coated materials,[10] have been proposed as in

[a]Corresponding authors: jose.martinez-gonzalez@ucd.ie, niall.english@ucd.ie

vivo bio-materials. When these materials are introduced into the body, the external part interacts with water, and a specific aqueous interface is created.

The dynamical behaviour of interfacial water with TiO_2 and SiO_2 has been probed by various spectroscopic methods[11–15] including neutron scattering (inelastic, quasielastic and backscattering) and infrared spectroscopy. Attenuated Total Reflection-Infrared (ATR-IR) spectroscopy has been used to monitor the growth of different water layers on a SiO_2 surface.[16] Quasi-elastic neutron scattering experiments have been used to study confined surface water in different materials[11,17] evaluating the vibrational density of states (VDOS), which can be used for the characterisation of the strength of hydrogen bonds,[16] providing information about the mobility of this interfacial water. However, information of local H-bond dynamics (formation and breaking) cannot be obtained with these techniques. In order to unravel the interaction among the atoms forming the outermost surface and water molecules in contact with them, theoretical techniques are required.

VDOS can be obtained through theoretical approaches[18] such as molecular dynamics (MD). From MD simulation of water, the velocity autocorrelation function can be extracted, the Fourier transform of which gives the power spectra or VDOS.[18] Moreover, through MD simulation, the IR spectra of water can be obtained via the dipole approach.[19]

Silicon and silicon-based materials has been studied via MD in numerous studies.[20,21] The wetting behaviour of different silicon surfaces has been attempted via molecular dynamics,[22–24] by simulating how a drop of water comes into contact with the surface, obtaining the three dimensional structure of the water droplet and calculating the contact angle of the drop of water with the surface. Ramos-Alvarado et al proposed improvements in the methodology for obtaining the contact angle that allow the calculation of the binding energy to the adhesion process that occurs in the interface. In these studies non-flexible water models were employed, however, the introduction of the bond flexibility in the water models[25] improve the calculation of dielectric constant and the pressure-temperature density behaviour obtaining values close to the experimental ones.[26] Specifically, the SPC/Fw[25] model has been developed to improve one of the most used models in simulations of biosystems, the simple point charge (SPC) model,[27] improving the description of dynamic and electrostatic properties without adversely influencing other properties.[25]

The present study investigates, for the first time, the dynamical properties of interfacial water in contact with silicon, hydrogen and hydroxyl terminated silicon-(100) surfaces, using MD. These surfaces have been chosen because they represent different types of behaviour when they are in contact with water. The surface ending in hydrogen is ours most hydrophobic, while the hydroxyl-terminated surface is hydrophilic and the silicon has a moderate hydrophobicity. The water density profiles, which have been obtained from the simulations, are related to the hydrophobic performance of the surfaces. This behaviour can also be seen in the study of the features of velocity density of states (VDOS) and infrared (IR) spectra obtained, which have been studies for the first monolayer in immediate contact with these surfaces. The analysis of these spectra shows that the molecules of water in this first layer have characteristics intermediate between solid/frozen water (ice) and structural organization characteristic of ambient-temperature liquid water. These data provide a closer view of the interface that occurs when a material is in contact with liquid water.

II. MATERIALS AND METHODS

A. Molecular-dynamics simulation details

Three-dimensional silicon-based surfaces, terminated by silicon, hydrogen and hydroxyl moieties, were constructed. The silicon surface consists of a 1 x 1 x 2 supercell of diamond structure of silicon lattice, with a 100 face along the laboratory *x*-*y* plane; the unit-cell constant, *a*, was 15.6 Å, corresponding to 254 Si atoms in total with 1 x 1 x 2 replication. This silicon surface was modified at the ends by adding a hydrogen-atom layer, to form the hydrogen-terminated surface, or by adding a hydroxyl layer to form the OH-terminal surface. Each surface was solvated by adding 378 water

molecules in contact therewith, with the bulk liquid-water layer having a density of 1 g/cm^3. The direction of heterogeneity was along the laboratory z-axis. The final dimensions of the cell were 15.6 x 15.6 x 69 Å. Further, in order to ascertain how simulation-box size may affect results, this simulation box was replicated along the x-y plane on 2 x 2 and 3 x 3 bases, whilst preserving the z-axis dimension; this led to respective larger-system simulation-box dimensions of 31.2 x 31.2 x 69 Å and 46.8 x 46.8 x 69 Å.

The Tersoff potential[28–30] was applied to the surfaces and flexible SPC-type model to water (SPC-FW).[25,27] All surfaces, and silicon atoms, were fully mobile. Silicon/water-oxygen, (Ow), surface-hydrogen (Hs)-Ow and surface-oxygen (Os)-Ow parameters were set to those of the SPC-FW Lennard-Jones potential. The binding energy of oxygen and silicon was modified using the value obtained by Pham et al[31] so as to model hydrophobic behaviour measured by previous experiments.[32] Only charge for Hs, Os and silicon connected with hydroxyl (Ss) was assigned. Comparison between different surfaces is enabled, because, in the case of the hydrogen-terminated silicon-(100) surface and the silicon-(100) surface, the importance of charges is minimal. In the case of the silicon surface, point charges cannot be assigned to the atoms, given its bare metal nature. For the hydrogen-terminated surface, this has been found to impart greater stability and inertness, since the silicon atoms are saturated. These values are summarised in Table I.

The Ewald method[33] was used to handle long-range electrostatics to within a relative precision of 10^{-6}, as implemented in DL_POLY v2 package.[34] MD was performed under three-dimensional periodic boundary conditions in a Nosé-Hoover NVT ensemble[33] at 300 K using velocity-Verlet integration with a 0.2 fs timestep, so as to sample adequate high-frequency vibration

TABLE I. Optimised parameters for the simulations. The values for Tersoff potential and interatomic parameters surfaces has been compiled from ref. 29, 30.

Optimised Tersoff potential for Silicon surfaces:			
	Si	O	H
A(eV)	1.8308 x10^3	1.88255 x10^3	86.7120
B(eV)	4.7118 x10^2	2.18787 x10^2	43.5210
γ (Å^{-1})	2.4799	4.17108	3.7879
μ(Å^{-1})	1.7322	2.35692	1.9800
β	1.1000 x10^{-6}	1.1632 x10^{-7}	4.0000
n	7.8734 x10^{-1}	1.04968	1.00
c	1.0039 x10^5	6.46921 x10^4	0.00
d	1.6217 x10^1	4.11127	1.00
h	-5.9825 x10^{-1}	-8.45922 x10^{-1}	1.00
R(Å)	2.5	1.7	0.80
S(Å)	2.8	2.0	1.00
Tersoff interatomic parameters (χ)			
Si	1.00	1.18	0.78
O	1.18	1.00	1.00
H	0.78	1.00	1.00
Van der Waals Potential (Lennard-Jones potential)			
i-j		ε_{IJ} (eV)	σ (Å)
Si(Ss)-Ow		0.1208781	2.6305
Ow-Ow		0.00674	3.166
Os-Os		0.0073719	3.07
Os-Ow		0.0070484	3.3625
Si-Os		0.1264269	2.5825
Van der Waals Potential (12-6 potential)			
i-j		A(eV·Å^{12})	B(eV·Å^6)
Si(Ss)-Hs		8209.2872	10.6282

of water hydrogen (Hw) atoms. For all cases and system sizes, the simulation was performed for 200 ps. In the case of the system based on the original 1 x 1 x 2 silicon cell, a 2 ns simulation was also performed with the aim of studying the formation and stability of solvation layers formed.

B. Axial water distribution and density

The distribution function of the oxygen atoms along the laboratory z-axis was calculated to establish the variation of water density along this axis. This axial distribution of density is related to the formation of the interface, water-surface, as well as on the different layers of solvation that are formed near the surface. In addition, variations in density peaks, or distances at which they occur, may offer clues as to the hydrophobicity or hydrophilicity of surfaces; this, in turn, may be interesting from the point of view of elucidation of structures that are formed at the different interfaces.

C. VACF analysis and IR spectrum

The infrared spectrum was obtained via dipole-based autocorrelation functions (ACFs). The normalised velocity-ACF of an atom, *j*, (or particular group of atoms, α), Z (t), is:[27]

$$Z^{\alpha}(t) = \langle v_j^{\alpha}(t) \cdot v_j^{\alpha}(0)\rangle / \langle v_j^{\alpha}(0) \cdot v_j^{\alpha}(0)\rangle \tag{1}$$

where brackets denote ensemble averaging and *i* denote the atom. The VDOS is the real part of the numerical Fourier transform of the (V)ACF; the underlying frequencies modes, *ω,* characteristic of time-variation may be gleaned therefrom.[27] The normalised VDOS (or power spectra) of the oxygen and hydrogen atoms in water were evaluated as:

$$Z(\omega) = \int_0^{\infty} Z^{\alpha}(t) \cos(\omega t)\, dt. \tag{2}$$

The oxygen atoms in water dominate translational motion, whilst hydrogen atoms reflect librational motions.[35]

The infrared (IR) absorption spectrum for the water boxes was obtained from the system-dipole-moment ACF via Fourier transformation as:[19,36,37]

$$I(\omega)\, \alpha \int_0^{\infty} \langle M(t) \cdot M(0)\rangle \cos(\omega t)\, dt \tag{3}$$

where I(ω) is the spectral density, M(t) is the total dipole moment of system at time *t*, and *ω* is the vibration frequency. M(t) is obtained as the vector sum of all individual molecular dipole moments of the water molecules in the simulation box[19,36]

$$M(t) = \sum_{i=1}^{m} \mu(t) \tag{4}$$

where μ(t) is the dipole-moment vector of the *i*th molecule at time *t* and *m* is the number of molecules in the simulation box. The ACF of the dipole moment is given by[38,39]

$$\langle M(t) \cdot M(0)\rangle = \langle \sum_{j=1}^{n} e_j r_j(t) \cdot \sum_{j=1}^{n} e_j r_j(0)\rangle \tag{5}$$

where *n* is the number of all atoms in the water box, e_j is the fixed electrical charge of the *j*th atom, and $r_j(t)$ is the position vector of the *j*th atom at time *t*.

The IR spectrum for the first adsorbed water monolayer the can be also obtained using the electrical flux-flux autocorrelation function[38]

$$\langle \sum_{j=1}^{n} e_j v_j(t) \cdot \sum_{j=1}^{n} e_j v_j(0)\rangle = \langle \sum_{j=1}^{n} e_j \frac{dr_j(t)}{dt} \cdot \sum_{j=1}^{n} e_j \frac{dr_j(0)}{dt}\rangle = \langle \frac{dM(t)}{dt} \cdot \frac{dM(0)}{dt}\rangle \tag{6}$$

which corresponds to the ACF of the time derivative of the dipole moment.[39] The spectral density is then calculated as:[38,40,41]

$$I(\omega)\, \alpha \int_0^{\infty} \langle \frac{dM(t)}{dt} \cdot \frac{dM(0)}{dt}\rangle \cos(\omega t)\, dt = \int_0^{\infty} \langle \sum_{j=1}^{n} e_j v_j(t) \cdot \sum_{j=1}^{n} e_j v_j(0)\rangle \cos(\omega t)\, dt. \tag{7}$$

The IR spectra of water at different temperatures have been calculated using the dipole auto-correlation function. However, to calculate the spectra of the water-silicon interface only the water molecules that spend 90% of the time in this interface will be taken into account. Therefore and given

that the calculated IR spectrum using the flux-flux autocorrelation function differs from IR spectrum obtained by the autocorrelation function only in its intensity[38] and, is less sensitive to the size of the sample to compute the IR,[42] we have used the latter formulation (flux-flux ACF) in the present study for calculating the IR spectrum.

III. RESULTS AND DISCUSSION

A. Ice, low-temperature and ambient-temperature liquid water

Classical molecular dynamics simulations were carried out according the procedure outlined above. For water, we simulate approximately 20 x 20 x 20 Å dimension water box, containing 216 molecules at 300 K (ambient temperature) and 220 K (low-temperature). For ice, we simulated 533 water molecules in a Hayward-Reimers I*h*-system in an approximately 45x45x45 Å-dimension box.

Figure 1 shows the vibrational density of states (VDOS) for hydrogen and oxygen. The VDOS spectra may be divided according to regions of stretching, bending and translational-librational components. The range for translational movement is less than 500 cm^{-1} for oxygen and around 400 to about 1000 cm^{-1} for hydrogen, respectively. Water bending contributes to a sharp peak at 1450 cm^{-1}, whilst the O-H stretch is represented as two sharp peaks between 3540 to 3696cm^{-1}.[43] A shoulder between 100 and 275 cm^{-1} could be observed in the ice and liquid water at 220 K. This shoulder was related with a decreasing in the mobility of the water molecules, which implies an increase of the structural organisation. In the case of ice, which has a clearly defined structure, this shoulder is clearly seen.

Figure 2 shows the infrared spectra obtained for ice and water (220 and 300 K) using the dipole approximation. There are three absorption regions, a group of peaks between 250 to 500 cm^{-1} due to the libration motions, a single peak approximately at 1450 cm^{-1} due the H-O-H bending vibration and two sharp peaks between 3540 to 3696 cm^{-1} region due the O-H stretching vibration. The position of these bands was similar that regions we found in VDOS spectra. However, the shoulder found in the power spectra has not been found. This may be because the intensity associated with this vibration is very small in the IR spectrum. In this case, the position of the peaks of the bands of bending and stretching was analysed in order to find some relation with the decrease in movement of the water molecules that can be correlated with the increase in structure.

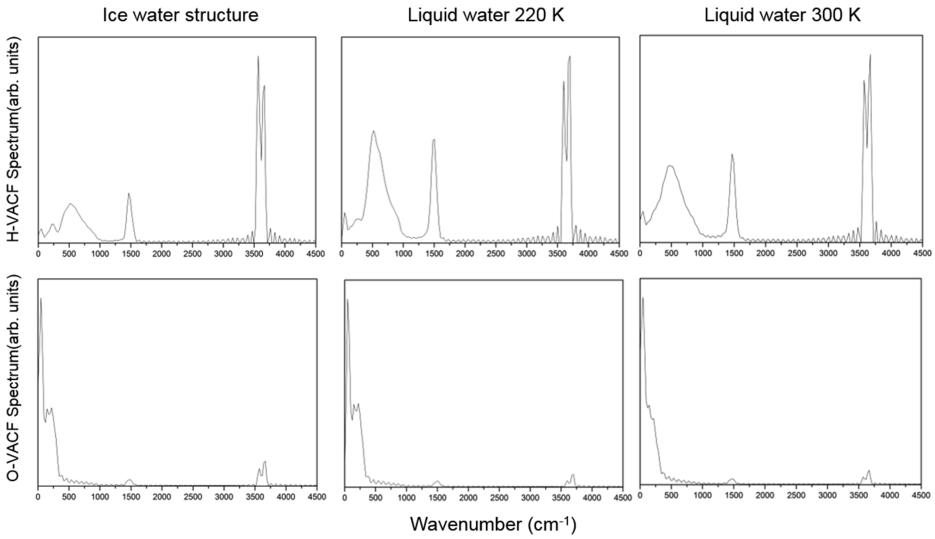

FIG. 1. Power spectra for ice (left) and liquid water at 220K(centre) and 300K (right). Hydrogen atoms (up), and oxygen atoms (down).

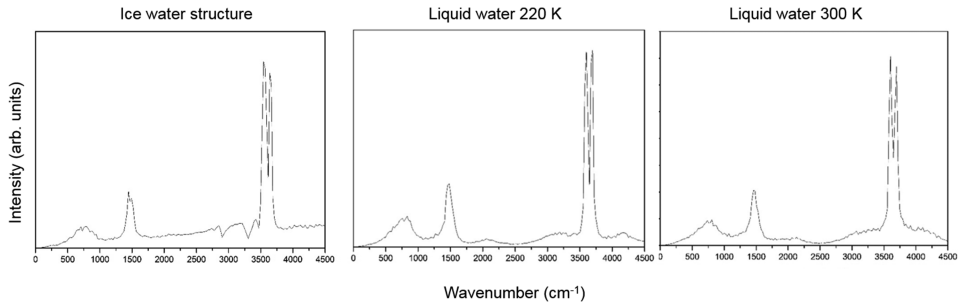

FIG. 2. Infrared Spectra of ice and liquid water at 220K and 300K.

TABLE II. Main peak position for ice, liquid water at 220K and liquid water at 300K.

		Ice (220K)	H_2O (220K)	H_2O (300K)
ν_s	Asym (cm^{-1})	3639	3696	3696
	Sym (cm^{-1})	3544	3600	3600
ν_b (cm^{-1})		1443-1490	1481	1481

It readily evident from Table II that the water-bending and stretching peaks are redshifted in the case of Ice-Ih structure. This shift was previously described[44,45] and it is related to the restrictions of movement that occurs when atoms were in an organized environment.[46] In the case of liquid water, at 300 or 220 K, the positions of the peaks are the same. This can be explained because there was not enough time for low-temperature water to undergo homogeneous nucleation water molecules at 220 K begin to grown like an ice-Ih crystal.[47] However, the simulation of water at 220 K provides an intermediate stage between both: the VDOS data in Fig 1 exhibits similarities with the ice-structure and IR spectrum in Fig 2 obtained with liquid water at 300 K.

B. Silicon

In order to identify the physically adsorbed water molecules, as well as the layers that form, a study was made of how the water density varied during the simulation across the laboratory z-axis. The variation of water density along the z-axis can be seen in Figure 3. The silicon-(001) surface lies between -28 to -12 Å along the z-axis of the cell. The water molecules solvated the surface both from above and below. The two faces of the surface produced a similar profile in the variation of the density. In order to clarify, for only the 'up' side, z-axis coordinate values greater than -20 Å, i.e. the silicon surface core where the water cannot enter, have been considered in the analysis.

Figure 3 shows two peaks near the two faces of the silicon surface. These peaks are related to the interface water-silicon; the first peak (d=1.35 g/cm^{-3}) is the zone with greater interaction with the surface, whilst the second (d=1.09 g/cm^{-3}) is a transitional zone with bulk water (d=1.00 g/cm^{-3}). The water density profile obtained is similar to previously obtain by theoretical studies for the wettability of this surface.[24] This indicates to us although the rigid models of water are sufficient for a description of this processes, they are not it when we want to obtain properties related to the vibrations of the links like VDOS and IR spectra. Due to the diffusion of water molecules, only the in this first layer have been used to obtain the dynamical properties of the adsorbed molecules of water (VDOS and IR spectra). Time intervals of 20ps were used throughout the dynamics, due to the fact that there are no water-molecule chemisorption events at the surface (ipso facto, given the non-dissociative nature of the water potential used). All calculated spectra correspond to one-time windows, unless otherwise indicated. This also allows monitoring if spectrum varies over time, and identification of when the first layer becomes fully formed when no changes are seen in the spectrum of VDOS.

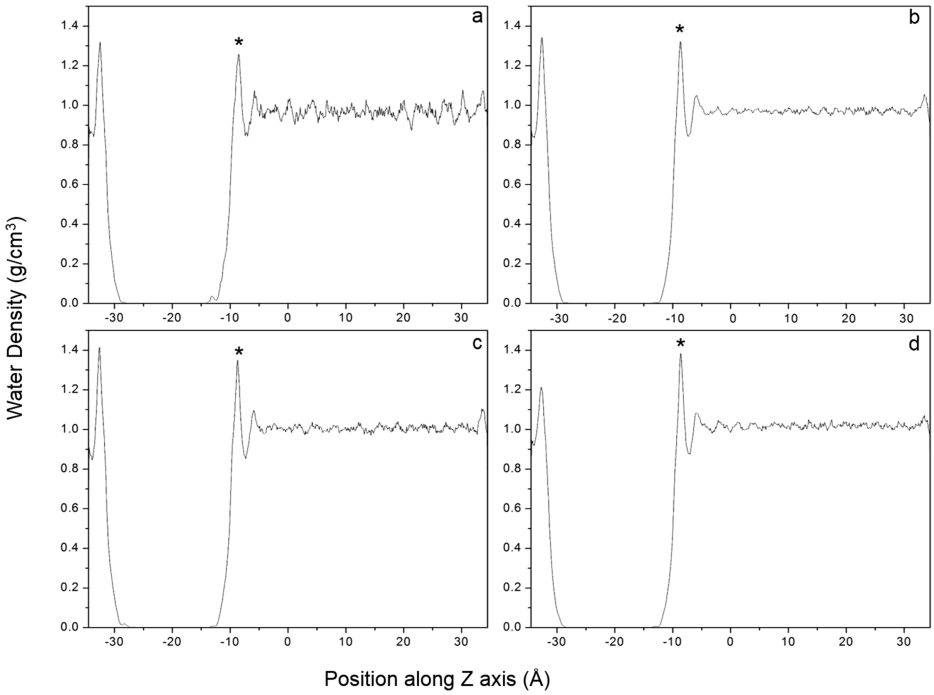

FIG. 3. Density distribution of water molecules surrounding the silicon cells 1x1x2 after 200ps (a), and after 2 ns (b), cell 2x2x2 (c) and cell 3x3x2(d). The asterisk indicates first solvation layer.

The VDOS spectra for first monolayer of water hydrogen and oxygen atoms are shows in Figure 4 after 200ps and 2 ns for the 1x1x2 supercell, and after 200ps for the 2x2x2 and 3x3x2 cases. For the 1x1x2 cell, a broad band is formed near 250 cm^{-1} in the VDOS of H. In the case of the oxygen, this is more difficult to see, but there is a substantial variation in the intensity at the same region. For the 2x2x2 and 3x3x2 cells, it is not easy to see the broad-band formation in the case of the hydrogen; however, it is very clear in the case of the oxygen. It could be conjectured that having a larger surface would require dynamics of longer duration that would stabilise this first solvation layer and allow the formation of a more stable structure over time. These broad bands have already been seen in the case of the VDOS ice and 220 K water spectra (Fig 1). Possibly, and due to the size of the monolayer, the shape of the corresponding VDOS are similar to those of the cooled water, wherein a subset of

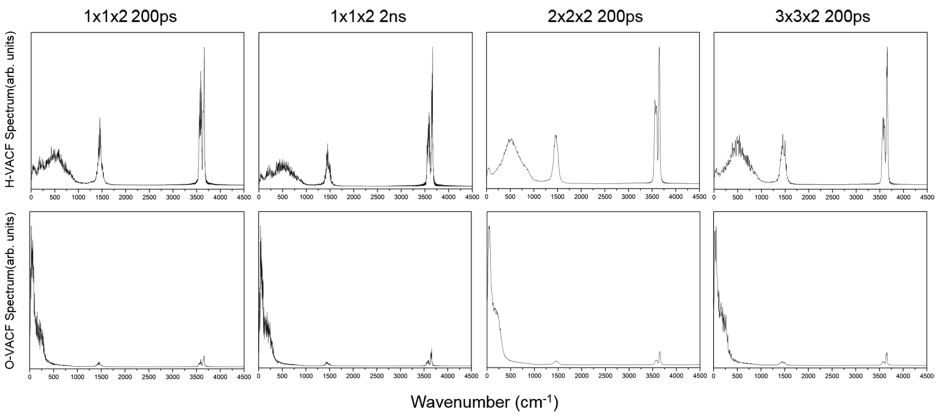

FIG. 4. Power spectra for silicon 1x1x2 cell (after200ps and 2ns), 2x2x2 cell and 3x3x2 cell. Hydrogen atoms (upper) and oxygen atoms (down).

the water molecules are intermediate between liquid and ice, and begin to form an ice-like ordered structure. However, the diffusion of the water molecules will interfere when extracting a VDOS, but having 90% sampling over the time interval assists with this.

The IR spectra calculated using equation (7) after 200ps for all cell sizes and after 2ns for the1x1x2 cell are shown at Fig 5. As seen in the previous section, the IR spectra has three absorption bands, at lower frequencies (under 1000 cm^{-1}) for librational motions, at 1450 cm^{-1} due the H-O-H bending vibration and between 3500 to 3700 cm^{-1} region due the O-H stretching vibration, which consists of two sharp peaks.

In this case it is not clear which is most representative IR spectrum shape from the four that are shown. If only the shape and the intensity of the IR spectrum are considered, two cases have been found. One in which a single peak appears in the bending vibration and the asymmetric stretching vibration is greater in intensity than the symmetrical one, and another case in which the bending band appears resolved into smaller band and the symmetrical stretching has a greater intensity than the asymmetrical. Therefore, we focus on the position of the main peaks of the bands. Table III shows the positions of the main peaks for the different supercells.

Comparing the data obtained in Table III with those previously proposed as reference structure of liquid and ice (cf. Table II), the values obtained for the highest-intensity peak for each vibration band were in an intermediate position between liquid water and ice. In the case of the ν_s asymmetric peak (around 3649 cm^{-1}), this is closer to ice values than liquid water for all cells. However in the case of the obtained ν_s symmetric peaks position, these are dispersed. This could be due to both diffusion processes between the different layers of water as that the structure not be fully defined, one intermediate step between both. For the bending peak position, scattered values can also be found; however, these values in general are at lower frequencies than those found for liquid water. With the data generated, it can be inferred that the structure of water molecules that spend more than 90% of each time interval at the silicon/water interface exhibit an organisation and dynamical behaviour similar to that of ice, albeit not fully. This can be due, on the one hand, to diffusion processes. On the other hand, the length of the window in which the analysis was performed may also play a rôle: 20 ps is a compromise to obtain a statistically sampling in the first solvating layer (Fig. 3). All attempts to use larger temporal window makes the analysis more complicated and substantially more statistically challenging. If we compare our results with the IR spectra obtained by Asay et al[16] using an humidity cell that controls moisture and allows a controlled growth of the silica-water interface we find that qualitatively they have some similarity. These ATR-IR spectra suggest that the water present in the same has an organization similar to that of ice.

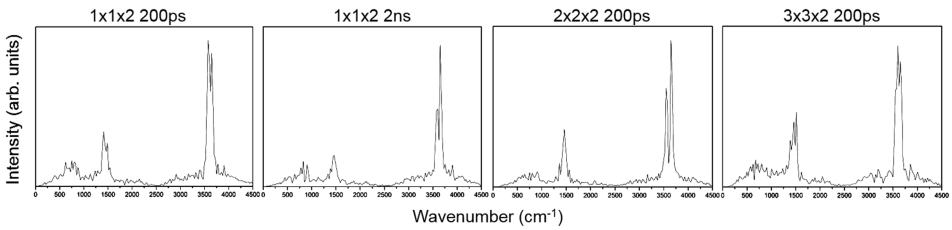

FIG. 5. IR spectra for the observed water monolayer's in contact with the silicon 1x1x2 cell (after 200ps and 2ns), 2x2x2 cell and 3x3x2 cell.

TABLE III. Main peak position for silicon 1x1x2, 2x2x2 and 3x3x2 supercells.

		1x1x2 (200ps)	1x1x2 (2ns)	2x2x2	3x3x2
ν_s	Asym (cm^{-1})	3649	3649	3649	3649
	Sym (cm^{-1})	3573	3579	3547	3598
ν_b (cm^{-1})		1443-1480	1462	1462	1513-1462

C. Hydrogen-terminated silicon

In the same way as in the previous case, a study of the variation of the density along the z-axis was made to identify the different layers of solvation that are generated near the hydrogen terminated silicon surface. The variation of water density can be seen in Figure 6. The surface was between -28 to -12 Å in the z-axis of the cell with water molecules solvating the surface both above and below.

A similar density profile, as shown for the previous surface, with a main peak (d = 1.5 g/cm^{-3}) close the faces of the surface and the generation of a second peak (d = 1.15 g/cm^{-3}). The values of the density in these peaks are higher than what had been shown previously. Also the size of the first layer, between the position of the hydrogen atoms of the surface and the position of the first peak, increased from 3.4 to 4.3 Å. This expansion of the first layer may be due to the hydrophobic properties of this type of surface. In case of the 3x3x1 supercell, a third solvation layer was evident, which shows a growth interface to almost 12 Å from the hydrogen in the surface.

Using the same criterion as before, molecules of water that spend almost 90 % of the time in this first layer, have been used to obtain the dynamical properties, VDOS and IR spectra. The VDOS spectra for first monolayer of water hydrogen and oxygen atoms after 200ps and 2 ns for the 1x1x2 cell, and after 200ps for the 2x2x2 and 3x3x2 supercells are shown in Figure 7.

For the 1x1x2 cell after 200ps a broad band is formed near 250 cm^{-1} in hydrogen and oxygen VDOS, as shown previously in Fig. 4. For the other VDOS-H spectra, the formation of a wide band is less evident which is similar to the VDOS-H for liquid water. However, in the case of the oxygen atoms (the translational spectra), the shape is roughly halfway between the ice and liquid water. For larger cells, the spectrum indicates that in the case of the interface, it is similar to what is found for the previous case, the silicon surface.

These spectra, which are intermediate between the ice spectrum and low-temperature water at 220 K, have been formed in a larger volume than in the previous more hydrophilic case, which, together with the phenomenon of diffusion, renders it slightly more challenging and complicated to obtain a spectrum of better statistical quality.

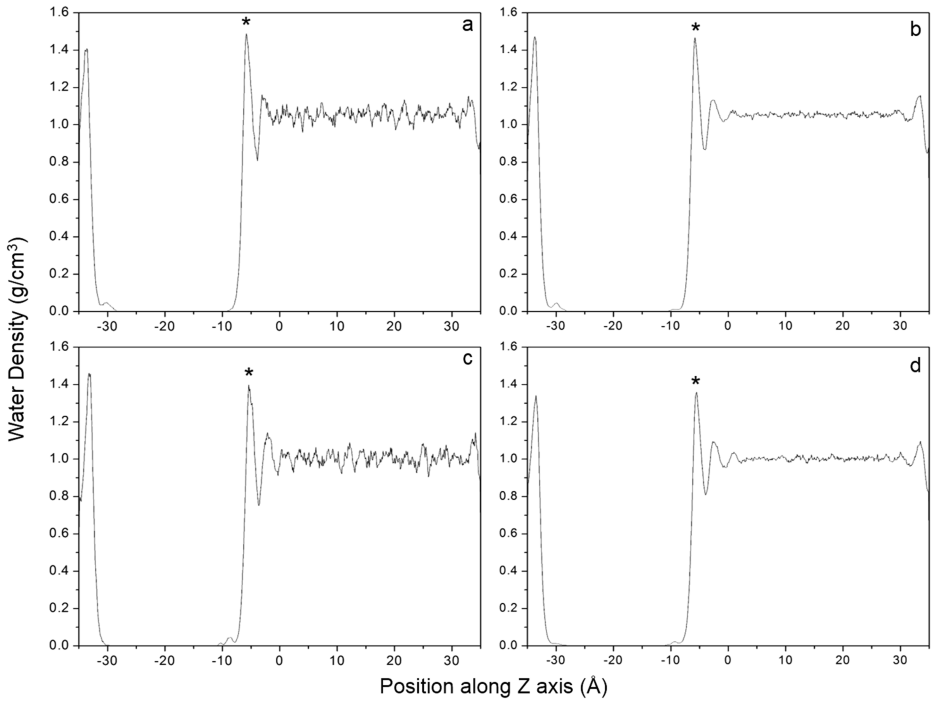

FIG. 6. Density distribution of water molecules surrounding the hydrogen terminated silicon 1x1x2 after 200ps (a), and after 2 ns(b), cell 2x2x2 (c) and cell 3x3x2(d). The asterisk indicates first solvation layer.

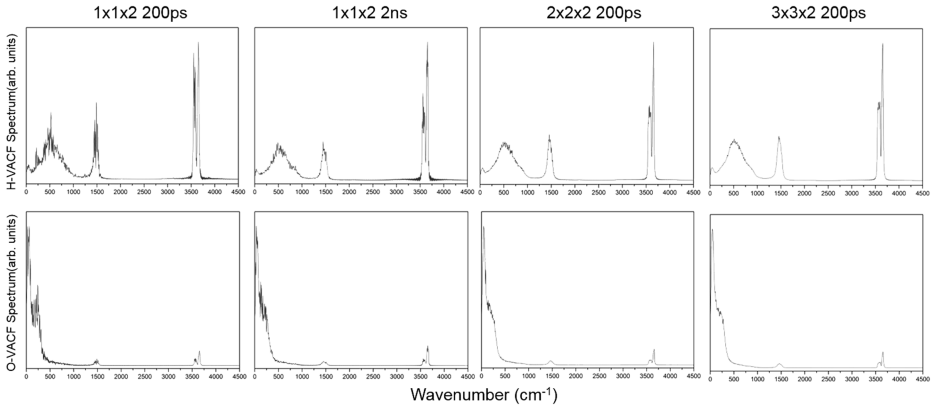

FIG. 7. Power spectra for the observed water monolayer's hydrogen atoms (upper) and oxygen atoms (down) in the case of the hydrogen terminated silicon 1x1x2 cell (after 200 ps and 2 ns), 2x2x2 and 3x3x2 supercells.

The electrical-flow ACF was calculated in order to obtain the IR spectrum for these interfaces. Figure 8 shows the IR spectra calculated for all cell sizes after 200 ps of simulation and after 2ns in the 1x1x2 cell case. Three main absorption bands have been shown, under 1000 cm^{-1} for librational motion, at 1450 cm^{-1} for the bending vibration and the O-H stretching vibration, where two peaks related to symmetrical and antisymetrical vibration appear between 3500 to 3700 cm^{-1}.

The shape for these spectra are similar between them, except in the bending band after 2 ns, where there are some minor differences. The positions of the main peaks of the bands are shown in Table IV.

The values obtained for the highest intensity peak for each vibration were in an intermediate position between liquid water and ice. Also, the stretching vibration (ν_s) values are similar to those obtained in the case of the silicon structure. The bending position (ν_b) frequency values are lower than for the silicon structure. This ν_b values are similar to ice structure values; besides a similar qualitative shape, several peaks appear at varying intensity, which is characteristic of a structure that is not fully defined. This is in line with the above, in that at the silicon/water interface, the water molecules display intermediate organisation between the defined structure of ice and liquid water.

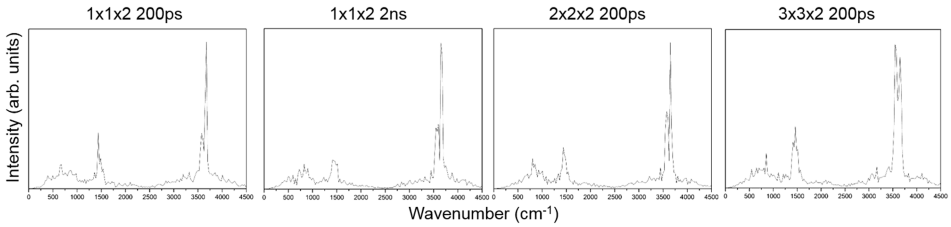

FIG. 8. IR spectra for the observed water monolayer's in contact with the hydrogen terminated silicon 1x1x2 cell (after 200 ps and 2 ns), 2x2x2 and 3x3x2 supercells.

TABLE IV. Main peak position for hydrogen terminated silicon 1x1x2, 2x2x2 and 3x3x2 cells.

		1x1x2 (200ps)	1x1x2 (2ns)	2x2x2	3x3x2
ν_s	Asym (cm^{-1})	3675	3649	3649	3649
	Sym (cm^{-1})	3573	3598	3573	3547
ν_b (cm^{-1})		1437	1437	1437	1462

D. Hydroxyl-terminated silicon

The study of the variation of the density along the z-axis has been carried out for the different hydroxyl-terminated silicon surfaces. This variation in the density allows identifying the different layers of solvation near the surface. Figure 9 shows the variation of water density along the z-axis. Again, the surface was between -28 to -10 Å along the z-axis of the cell, with water molecules solvating the surface both faces.

The density profiles obtained for all cells are similar, but different from the other surfaces. The two main peaks (d = 2.0-1.8 g/cm^{-3}) are closer the surface (0.6 Å from the hydrogen atom of the hydroxyl). The second peak (d = 1.5-1.7 g/cm^{-3}), reached a distance of 4.7 Å, similar to the main peak in hydrogen-terminated silicon surface. In the 2x2x2 cell, a third solvation layer has been formed, which ends at a distance of 8 Å from the hydrogen. The value of density at the main-peak is the highest of all systems considered. The size of the first layer is related to the formation of hydrogen bonds between the water molecules and the surface. In this case, the distinct hydrophilic effect of the hydroxyls can be seen. With this data, and following the criterion of permanence at the temporary interface (first layer) already stated (90 %-plus over 20 ps), the VDOS and IR spectra form the dynamical properties have been obtained (cf. Figure 10).

After 200 ps, the VDOS of 1x1x2 supercell shows the absence of a broad band near 250 cm^{-1} in hydrogen, which appears in the previous spectra. This may be related to the adsorption of water molecules at the surface. However oxygen VDOS was similar to previous surfaces. The remaining VDOS spectra for hydrogen and oxygen are intermediate between the defined structure of ice and liquid water, like the other surfaces studied (cf. Fig. 4 and 7). Therefore according these results, at the interface between water and solid, water tends to adopt an organisation in part similar to the one it has when it freezes, and is consistent with the findings of ref. 18 for water-titania interfaces. The IR spectra for all of these interfaces are depicted in Figure 11, calculated using the electrical-flow approach. Again, three main absorption bands are present, i.e., the librational mode under 1000 cm^{-1}, the bending vibration at 1450 cm^{-1} and the O-H stretching vibration, with two peaks related to symmetrical and asymmetrical vibration, between 3500 to 3700 cm^{-1}. The shapes for these spectra

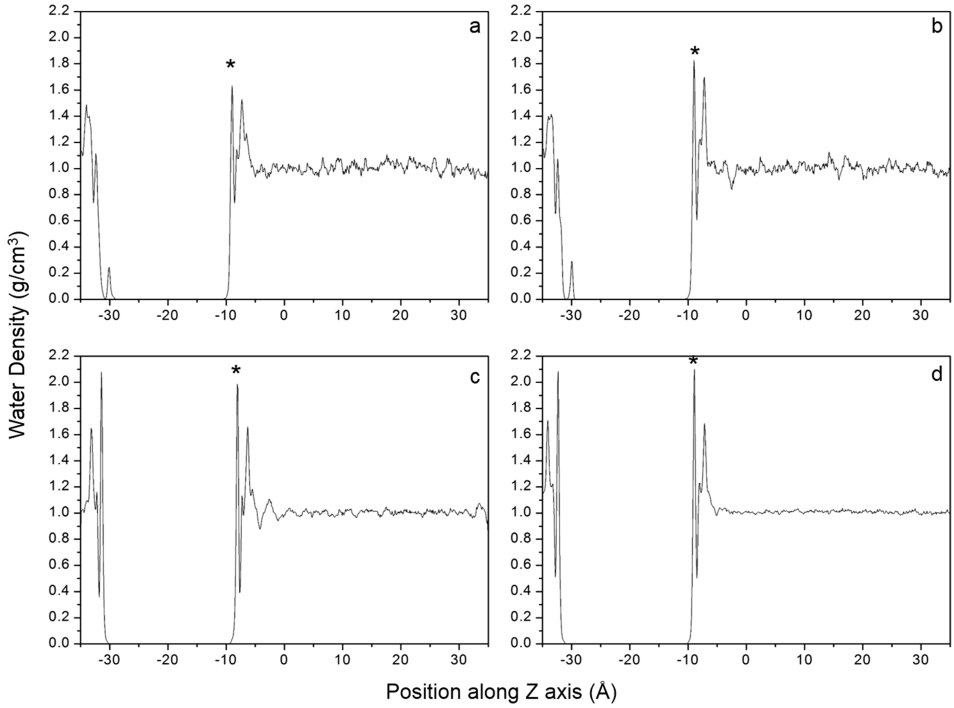

FIG. 9. Density distribution of water molecules surrounding the hydroxyl terminated silicon cells 1x1x2 after 200ps (a), and after 2 ns(b), cell 2x2x2 (c) and cell 3x3x2(d). The asterisk indicates first solvation layer.

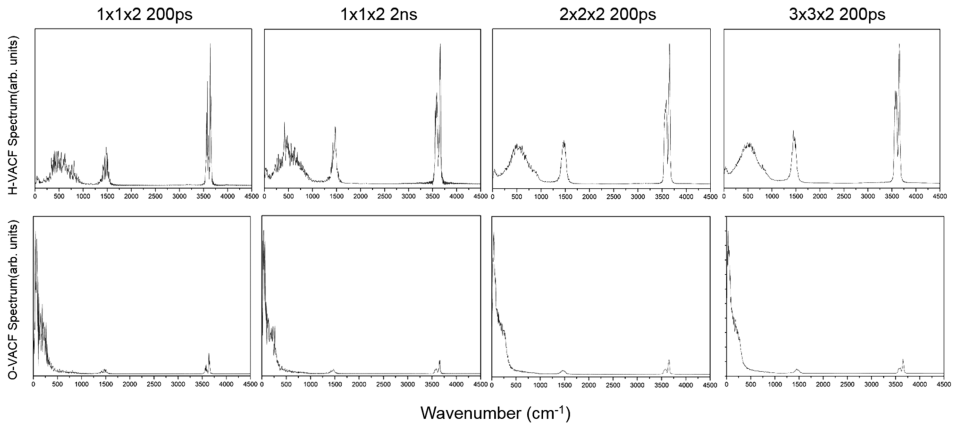

FIG. 10. Power spectra for the observed water monolayer's hydrogen atoms (upper) and oxygen atoms (down) in the case of the hydroxyl terminated silicon 1x1x2 cell (after 200ps and 2ns), 2x2x2 cell and 3x3x2 cell.

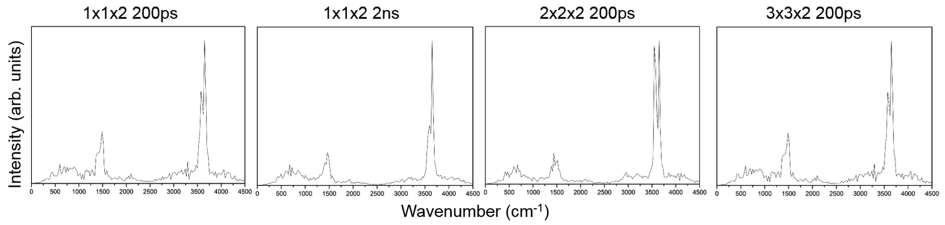

FIG. 11. IR spectra for the observed water monolayer's in contact with the hydroxyl terminated silicon 1x1x2 cell (after 200ps and 2ns), 2x2x2 cell and 3x3x2 cell.

are similar between them, although for the case of the 2x2x2 cell. The IR spectrum for this cell shows differences in the shape of the bending band, where the peak of higher intensity is at a lower frequency, as well as in the stretching band, where the intensities are similar for the symmetrical and asymmetric vibrations.

The positions of the main peak of the bands are shown in Table V. The values obtained for the highest-intensity peak for each vibration were in an intermediate position between liquid water and ice. Also, the stretching vibration (ν_s) values are similar to those obtained in the case of the silicon structure. The bending-position (ν_b) frequency is lower than for the silicon structure. This ν_b value is similar to ice-structure values, besides the similarity in shape; however, in the different cells, the ν_b shape appears as different peaks of varying intensity, which is characteristic of a structure that is not fully defined. This is consistent with the above findings, in that in the interface of the system, the water molecules have an intermediate organisation between the defined structure of the ice and the organisation that is in the liquid water.

The stretching asymmetric vibrations for all cells are close to the ice value (3639cm^{-1}). However the values for the stretching symmetric and bending vibration are more dispersed. In the case of ν_b, they appear between 1437 to 1487 cm^{-1}. In Table II, it can be verified that, for the case of the ice spectrum, the bending vibration appears between 1443 and 1490 cm^{-1}, whilst in the case of liquid water (both at 220 and 300K) the main value is 1481 cm^{-1} – confirming more ice-like dynamical

TABLE V. Main peak position for hydroxyl terminated silicon 1x1x2, 2x2x2 and 3x3x2 cells.

		1x1x2 (200ps)	1x1x2 (2ns)	2x2x2	3x3x2
ν_s	Asym (cm^{-1})	3649	3649	3649	3649
	Sym (cm^{-1})	3547	3598	3547	3573
ν_b (cm^{-1})		1487	1462	1437	1487

behaviour of the adsorbed monolayer. The shape of the hydroxyl terminated silicon spectra follow a pattern. In the case of the Vb, all cells have a main peak centred at 1487 cm^{-1} with the exception of the 2x2x2 cell. As for the Vs, in most cases, the asymmetric vibration is higher in relative intensity than the symmetric.

IV. CONCLUSIONS

MD simulations for silicon, hydrogen- and hydroxyl-terminated silicon displays water-density 'ordering' along the laboratory z-axis, dependant on the hydrophobicity of the different systems and the position of this first adsorbed layer. For instance, it has been found that both the position and the width of this layer is greater for the more hydrophobic material (H-terminated Silicon) than in the case of the hydrophilic materials. VDOS of the oxygen and proton and IR spectra of the first monolayer of adsorbed water, calculated via Fourier transformation, indicate similarities to more confined-pp, ice-like dynamical behaviour (redolent of ice). This is true of both hydrogen- and hydroxyl-terminated silicon surfaces at both 220 and 300K, and is consistent with previous findings discussed in the results section.

It was observed that good qualitative agreement is obtained between the VDOS for this first layer in all systems. Although there are differences between them, it can be said that the shape of the same in simulated vibrational bands is very similar. The VDOS for the lower-frequency zone indicates that for the interface studied (i.e., the first layer near the surface), the water molecules try to organise in a similar form, and that this form is intermediate between liquid water and ice for all the supercells.

For the case of the IR spectrum, the shape of the spectrum is very similar for all cell systems and sizes. Examination of the position of the highest-intensity peaks for the stretching and bending bands indicate that such water molecules in the first solvating layer are organised in intermediate fashion between ice and liquid water. This confirms what was found in the case of the VDOS spectra, calculated in the present study. Moreover, the simulation of the IR spectrum for the first solvation layer could help in the comparison with experimental spectra, and help to unravel how is the organisation and interaction of water molecules in contact with different materials.

ACKNOWLEDGMENTS

The authors acknowledge gratefully acknowledge funding from the European Union under the Framework Programme 7, as part of a European Research Council Starting Grant Programme (ERC-SG-335508 'BioWater'), and Dr. Zdenek Futera for some technical assistance with the creation of the initial structures and the obtaining of the parameters of the force fields.

[1] E. A. Vogler, Ad. Colloid Interfaces Sci. **74**, 69–117 (1998).
[2] H. R. Pruppacher and J. D. Klett, *Microphysics if clouds and Precipitation* (Kluwer Academic Publishers, The Netherlands, 1997).
[3] W. Stumm, L. Sigg, and B. Sulzberger, *Chemistry of the Solid-Water Interface at the Mineral-Water and Particle-Water Interface in Natural Systems* (Wiley, New York, 1992).
[4] B. L. de Groot and H. Grubmüller, Curr. Opin. Struct. Biol. **15**, 176–183 (2005).
[5] S. Margel, E. A. Vogler, L. Firment, T. Watt, S. Haynie, and D. Y. Sogah, J. Biomed. Mater. Res. **27**(12), 1463–1476 (1993).
[6] P. G. de Gennes, Rev. Mod. Phys. **57**, 827–863 (1985).
[7] M. Barisik and A. Beskok, Molecular Simulations **39**, 700–709 (2013).
[8] J. P. Nayak and J. Bera, Silicon **4**, 57–60 (2012).
[9] Q. Shabir, K. Webb, D. K. Nadarassan, A. Loni, L. T. Canham, M. Terracciano, L. De Stefano, and I. Rea, Silicon, 1–11 (2017).
[10] C. P. Stallard, K. A. McDonnell, O. D. Onayemi, J. P. O'Gara, and D. P. Dowing, Biointerphases **7**, 31(12) (2012).
[11] E. C. Spencer, A. A. Levchenko, N. L. Ross, A. I. Kolesnikov, J. Boerio-Goates, B. F. Woodfield, A. Navrotsky, and G. Li, The Journal of Physical Chemistry A **113**(12), 2796–2800 (2009).
[12] A. A. Levchenko, A. I. Kolesnikov, N. L. Ross, J. Boerio-Goates, B. F. Woodfield, G. Li, and A. Navrotsky, The Journal of Physical Chemistry A **111**(49), 12584–12588 (2007).
[13] E. Mamontov, L. Vlcek, D. J. Wesolowski, P. T. Cummings, W. Wang, L. M. Anovitz, J. Rosenqvist, C. M. Brown, and V. G. Sakai, The Journal of Physical Chemistry C **111**, 4328–4341 (2007).
[14] E. Mamontov, D. J. Wesolowski, L. Vlcek, P. T. Cummings, J. Rosenqvist, W. Wang, and D. R. Cole, The Journal of Physical Chemistry C **112**, 12334–12341 (2008).

[15] E. Mamontov, L. Vlcek, D. J. Wesolowski, P. T. Cummings, J. Rosenqvist, W. Wang, D. R. Cole, L. M. Anovitz, and G. Gasparovic, Physical Review E **79**, 051504(051506) (2009).
[16] D. B. Asay and S. H. Kim, The Journal of Physical Chemistry B **109**(35), 16760–16763 (2005).
[17] H.-W. Wang, M. J. DelloStritto, N. Kumar, A. I. Kolesnikov, P. R. C. Kent, J. D. Kubicki, D. J. Wesolowski, and J. O. Sofo, The Journal of Physical Chemistry C **118**(20), 10805–10813 (2014).
[18] R. S. Kavethekar, N. J. English, and J. M. D. MacElroy, Molecular Physics **109**, 2645–2654 (2011).
[19] A. R. Leach, *Molecular Modelling*, 2nd ed. (Pearson, Harlow, 2001).
[20] Y. Quin, Y. Chen, L. Liu, and G. Zhao, Proc. Inst. Mech. Eng. Part: J. Nanoeng. Nanosyst **226**, 31–34 (2012).
[21] J. Jingchum, S. liu, and X. Yang, Appl. Surf. Sci. **255**, 9078–9084 (2009).
[22] T. H. Yen, Mol. Simul. **37**, 766–778 (2011).
[23] M. Barisik and A. Beskok, Mol. Simul. **39** (2013).
[24] B. Ramos-Alvarado, S. Kumar, and G. P. Peterson, The Journal of Chemical Physics **143** (2015).
[25] Y. Wu, H. L. Tepper, and G. A. Voth, The Journal of Chemical Physics **124**, 024503–024512 (2006).
[26] G. Raabe and R. J. Sadus, The Journal of Chemical Physics **134**(23), 234501 (2011).
[27] M. P. Allen and D. J. Tildesley, *Computer Simulation of Liquids* (Oxford University Press, 1987).
[28] J. Tersoff, Phys. Rev. B **39**, 5566–5568 (1989).
[29] S. Munetoh, T. Motooka, K. Moriguchi, and A. Shintani, Computational Materials Science **39**, 334–339 (2007).
[30] F. de Brito Mota, J. F. Justo, and A. Fazzio, Journal of Applied Physics **86**, 1843–1847 (1999).
[31] A. T. Pham, M. Barisik, and B. Kim, Int. J. Prec. Eng. and Manufacturing **15**, 323–329 (2014).
[32] B. Arkles, Paint & Coatings Industry Magazine **22**, 114–135 (2006).
[33] N. J. English and J. M. D. Macelroy, Molecular Physics **100**, 3753–3775 (2002).
[34] W. Smith, T. R. Forester and I. T. Todorov, *The DL_POLY_2 User Manual*, v. 2.19 ed. (2008).
[35] J. S. Tse, M. L. Klein, and I. R. McDonald, The Journal of Physical Chemistry **87**, 4198–4203 (1983).
[36] B. Guillot, The Journal of Chemical Physics **95**, 1543–1551 (1991).
[37] B. Boršnik, D. Pumpernik, D. Janežič, and A. Ažman, *Molecular Interactions* (Willey, 1980).
[38] B. Boulard, J. Kieffer, C. C. Phifer, and C. A. Angell, J. Non-Cryst. Solids **140**, 350–358 (1992).
[39] P. Bornhauser and D. Bougeard, The Journal of Physical Chemistry B **105**, 36–41 (2001).
[40] M. Praprotnik, D. Janežič, and J. Mavri, The Journal of Physical Chemistry A **108**, 11056–11062 (2004).
[41] M. Praprotnik and D. Janežič, The Journal of Chemical Physics **122**, 174103(174110) (2005).
[42] J. Brawer, H. Schipper, and B. Robaire, Endocrinology **112**(1), 194–199 (1983).
[43] N. Kumar, S. Neogi, P. R. C. Knet, A. V. Bandura, J. D. Kubicki, D. J. Wesolowski, D. Cole, and J. O. Sofo, The Journal of Physical Chemistry C **113**, 13732–13740 (2009).
[44] W. M. Irvine and J. B. Pollack, Icarus **8**, 324–360 (1968).
[45] Y. Maréchal, J. Mol. Struc. **1004**, 146–155 (2011).
[46] T. A. Weber and F. H. Stillinger, The Journal of Physical Chemistry **87**, 4277–4281 (1983).
[47] M. Matsumoto, S. Saito, and I. Ohmine, Nature **416**(6879), 409–413 (2002).